Applied Thermal Engineering 122 (2017) 642–652

Contents lists available at ScienceDirect

Applied Thermal Engineering

journal homepage: www.elsevier.com/locate/apthermeng

Research Paper

Sensitivity analysis and multi-objective optimization of a heat exchanger tube with conical strip vortex generators

Nianben Zheng, Peng Liu, Feng Shan, Zhichun Liu, Wei Liu *

School of Energy and Power Engineering, Huazhong University of Science and Technology, Wuhan 430074, China

HIGHLIGHTS

- A modified conical strip vortex generator was proposed to enhance heat transfer.
- A sensitivity analysis was carried out.
- The optimum design parameters was obtained by NSGA-II and TOPSIS.
- The temperature and flow fields were presented and analyzed.

ARTICLE INFO

Article history:
Received 4 January 2017
Revised 10 April 2017
Accepted 9 May 2017
Available online 13 May 2017

Keywords:
Sensitivity analysis
Multi-objective optimization
Conical strip vortex generator
Thermal-hydraulic performance

ABSTRACT

This paper exhibited the results of sensitivity analysis and multi-objective optimization of a heat exchanger tube with conical strip vortex generators. The design parameters included the Reynolds number (*Re*), the conical strip filling ratio (*C*) and the pitch ratio (P^*), and the objective functions were the Nusselt number ratio and the friction factor ratio. The main aim of this study was to identify the optimum design parameters for the maximum heat transfer enhancement with the minimum pressure drop augmentation. Response Surface Methodology (RSM) was, firstly, applied to approximate objective functions. Based on RSM, sensitivity analyses of the responses to design parameters were carried out. Results indicated that both the heat transfer rate and the pressure drop increased with an increment in the conical strip filling ratio and Reynolds number and a reduction in the pitch ratio, but the pressure drop was more sensitive to these design parameters compared to the heat transfer rate. Furthermore, the Non-dominated Sorting Genetic Algorithm II (NSGA-II) was employed to optimize the objective functions, and the most compromising solution (i.e. $Re = 1468$, $C = 0.35$, and $P^* = 3.97$) was finally selected from the Pareto front attained by the multi-objective optimization. The associated Nusselt number ratio and friction factor ratio for this solution were 6.56 and 7.07, respectively. The findings of this work may provide practical guidelines for researchers to design efficient heat exchangers.

1. Introduction

With the ever-increasing need for efficient systems in many cases of thermal engineering, engineers and researchers have proposed and applied various techniques for heat transfer enhancement. By generating vortexes to disrupt the thermal boundary layer growth, vortex generators (VGs) such as twisted tapes [1,2], winglet vortex generators [3], and strip vortex generators [4] are one of the practical techniques to enhance the thermal behavior.

Generally, heat transfer behavior can be intensified considerably with the aid of vortex generators, but the pressure drop is also augmented dramatically. Some researchers have attempted to make a compromise between the heat transfer enhancement and pressure drop augmentation through multi-objective optimizations. Abdollahi and Shams [5] optimized the attack angle and outline of winglet VGs for heat transfer intensification by GA and ANN. Later they [6] applied the same method to examine the nanofluid flow in a tube with VGs. Liu et al. [7] achieved the optimal fin distribution to eliminate the contradictory between flow and thermal performance by mathematical optimization. The Taguchi approach was applied by Mamourian et al. [8] to determine the optimum conditions of heat transfer of nanofluid flow in a wavy surface square cavity. Recently, Damavandi et al. [9] utilized the Non-Dominated Sorting Genetic Algorithm II (NSGA-II) and computational fluid dynamics (CFD) to optimize the finned heat exchangers for maximum Colburn factor and minimum friction factor.

* Corresponding authors.
E-mail address: w_liu@hust.edu.cn (W. Liu).

http://dx.doi.org/10.1016/j.applthermaleng.2017.05.046
1359-4311/

Nomenclature

ANOVA	analysis of variances
C	conical strip filling ratio ($C = 3\alpha/2\pi$)
C_p	specific heat (J kg^{-1} K^{-1})
D	diameter of the tube (mm)
f	friction factor
f/f_0	friction factor ratio
L	length of the tube (mm)
Nu/Nu_0	Nusselt number ratio
P	pitch of the conical strips (mm)
P^*	non-dimensional pitch ratio ($P^* = P/D$)
p	pressure (Pa)
q	heat flux (W m^{-2})
R^2	coefficient of multiple determination
RSM	response surface methodology
T	temperature (K)
u	velocity (m s^{-1})

Greek symbols

α	the radian of the conical strip
θ	cone angle (°)
ε	error
μ	dynamic viscosity (kg m^{-1} s^{-1})
δ	thickness of the conical strip (mm)
ρ	density (kg m^{-3})

Subscripts

in	inlet
0	smooth tube
out	outlet
w	wall

Sensitivity analysis, which is a method to determine how the uncertainties in a model input affect the output for the model, has been applied in many fields of thermal engineering to find out the effective factors. Akbarzadeh et al. [10] performed a sensitivity analysis to examine the thermal and pressure drop characteristics of nanofluid flow in a wavy channel. It was found that the sensitivity of pressure drop to the channel aspect ratio was more than that of pressure drop to the Reynolds number and solid volume fraction. Mamourian et al. [11] evaluated the influence of vortex generators position on heat transfer and nanofluid homogeneity in a solar heat exchanger numerically. The results indicated that the nanoparticles concentration ratio was less sensitive than heat transfer to the design parameters. Later, Mamourian and his co-workers [12] investigated the MHD effects and inclination angles on natural convection heat transfer in a square cavity using Al_2O_3-water nanofluid though numerical simulations and sensitivity analysis. They found that the effect of Hartmann number on heat transfer and total entropy generation was negligible, and an increase in the inclination angle led to an increment of the sensitivity of heat transfer and total entropy generation to this angle. Milani Shirvan et al. [13] applied the porous media insert to enhance the heat transfer rate and effectiveness of a double pipe heat exchanger. Effects of Reynolds number (Re), Darcy number (Da) and the porous substrate thickness (δ) were studied. According to their results, the maximum heat transfer rate and effectiveness could be obtained for $Re = 5000$, $Da = 10^{-5}$ and $\delta = 1$. Later, Milani Shirvan et al. [14] numerically studied the mixed convection and radiation heat transfer of nanofluid flow in a solar heat exchanger using the two phase mixture model. Recently, Milani Shirvan and his co-workers [15] used the response surface methodology (RSM) to explore the natural convection and surface radiation heat transfer performance in a porous solar cavity receiver. They also presented the sensitivity analysis to determine the effective parameters. It was found that the mean Nusselt number of natural convection heat transfer was more sensitive than the mean Nusselt number of radiation heat transfer to Rayleigh number, porous substrate thickness, Darcy number and inclination angle. The same analysis method was applied by Milani Shirvan et al. [16] to examine the power output of a prototype solar chimney in Zanjan, Iran. Lately Mirzakhanlari et al. [17] analyzed the heat transfer enhancement and drag reduction of nanofluid flow in a lid-driven square cavity in which the effect of an inner rotating cylinder was considered.

Previous studies [18,19] have demonstrated that the conical strip vortex generator is a practical technique to increase the heat transfer rate for efficient systems. However, sensitivity analysis of the effective parameters on the flow and heat transfer behavior in a tube fitted with conical strip vortex generators has scarcely been considered in the open literature. To fill in this gap, in this work, sensitivity analysis of the effective parameters on the frictional and thermal performance in a tube fitted with the conical strip vortex generators was carried out using Responses Surface Methodology. The main aim of this study was to identify the optimum design parameters for the maximum heat transfer enhancement with the minimum pressure drop through a multi-objective optimization process. The findings regarding the proposed conical strip vortex generator of this work may provide practical guidelines for researchers to design efficient heat exchangers.

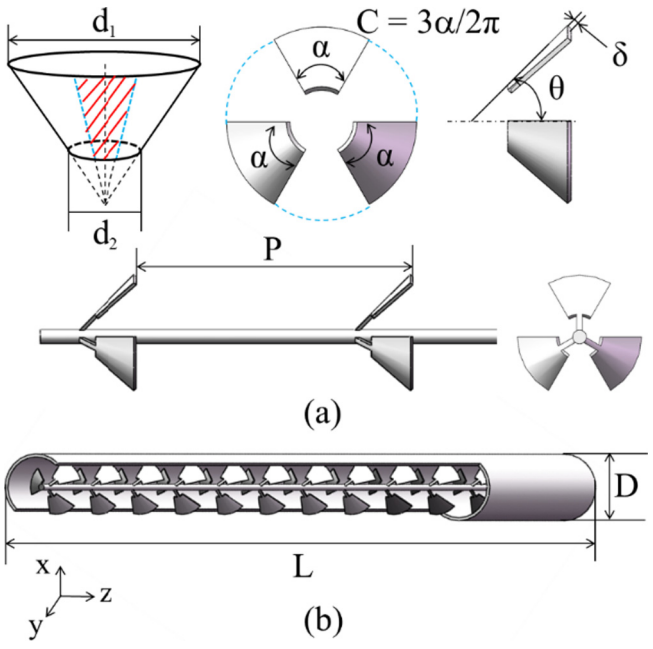

Fig. 1. Geometric details of the physical model: (a) conical strip vortex generators; (b) a tube inserted with conical strip vortex generators.

2. Physical model

Fig. 1 shows the conical strip vortex generator considered throughout this work. The vortex generator was mainly composed of the cone-shaped strips and a central rod. These strips were cut from a hollow circular truncated cone, which had a thickness (δ) of 0.5 mm and cone angle (θ) of 45°, and the radians of the strips were denoted by α. The bottom and top surfaces of the hollow circular truncated cone were ring-shaped, and their diameters were d_1 (d_1 = 6 mm) and d_2 (d_2 = 18 mm), respectively. These strips were uniformly attached to the central rod of 2 mm in both circumferential and axial directions using thin rods. P denoted the pitch of the conical strips along the tube. The vortex generator was inserted in a round tube that had a length (L) of 500 mm and an inner diameter (D) of 20 mm. To facilitate the investigation of the geometric parameters, we defined the conical strip filling ratio ($C = 3\alpha/2\pi$) and pitch ratio ($P^* = P/D$) as the ratios of the area of strips to that of a hollow circular truncated cone and the strip pitch to the tube diameter, respectively.

3. Mathematical model

3.1. Numerical methods

The commercial CFD software ANSYS Fluent 15.0 [20] was applied to perform the numerical simulation. The flow and heat transfer phenomenon considered throughout this paper was assumed steady, laminar, and three-dimensional. The properties of the working fluid (i.e. water) was held constant during the simulation. The governing equations in the Cartesian tensor form are given as follows [21].

$$\frac{\partial(\rho u_i)}{\partial x_i} = 0 \tag{1}$$

$$\frac{\partial}{\partial x_j}(\rho u_i u_j) = -\frac{\partial P}{\partial x_i} + \frac{\partial}{\partial x_j}\left[\mu\left(\frac{\partial u_i}{\partial x_j} + \frac{\partial u_j}{\partial x_i}\right)\right] \tag{2}$$

$$\frac{\partial}{\partial x_j}\left(\rho u_j C_p T - k\frac{\partial T}{\partial x_j}\right) = 0 \tag{3}$$

where k, ρ, μ, C_p are the thermal conductivity, density, dynamic viscosity, and specific heat, respectively. Also, T represents the temperature; p is the pressure, and u_i represents the component of velocity in the direction of x_i.

The fully developed temperature and velocity profiles [22] given by Eqs. (4) and (5) were specified at the inlet of the tube. A pressure-outlet condition (p_{out} = 0 pa, gauge pressure) was set up at the outlet. A constant and uniform heat flux of 2000 W/m^2 was assigned to the tube wall, and the no-slip condition was assumed at the surface of conical strip vortex generators and the tube wall.

$$u = u_c\left(1 - \frac{r^2}{R^2}\right) \tag{4}$$

$$T = T_c + \frac{qR}{k}\left[\left(\frac{r}{R}\right)^2 - \frac{1}{4}\left(\frac{r}{R}\right)^4\right] \tag{5}$$

where u_c represents the velocity at the centerline of the tube, and T_c is the temperature at the centerline of the tube. Also, q represents the heat flux; R is the tube radius, and r refers to the radial distance.

In this work, the double precision pressure based solver was applied for numerical simulation. To discretized the pressure term, the standard scheme was utilized. The second-order upwind scheme was used to discretize the momentum and energy terms. To handle the coupling between the velocity and the pressure fields, the SIMPLE algorithm was applied. The solution was considered to be converged when all the residues are less than a prescribed value of 10^{-6}. In addition, the net mass flux balance across the computational domain was checked to assist the evaluation of the convergence of the solution.

The definitions of main parameters are given as follows.

The definition of the average heat transfer coefficient (h) is given by:

$$h = \frac{q}{T_w - T_m} \tag{6}$$

where T_w represents the wall temperature, and T_m is the bulk temperature of water.

The Nusselt number (Nu) is expressed as:

$$Nu = \frac{hD}{k} \tag{7}$$

The definition of the friction factor (f) is:

$$f = \frac{\Delta P}{(L/D)\rho u^2/2} \tag{8}$$

where Δp represents the pressure drop, and u represents mean velocity along the tube.

The definition of Reynolds number (Re) is expressed as:

$$Re = \frac{\rho u D}{\mu} \tag{9}$$

Besides, Nu/Nu_0 and f/f_0 represent the Nusselt number ratio and the friction factor ratio, respectively. Note that the subscript '0' refers to the smooth tube.

3.2. Grid generation and independence test

As shown in Fig. 2, the computational domain was discretized by hybrid grids composed of prism grids, hexahedral grids, tetrahedral grids, and pyramids. More details about the grid generation can refer to [23]. Before proceeding further, a grid independence test should be done to make sure that the results are irrespective of the grid number. In this work, the tube with conical strip vortex generators with C = 1/2, and P^* = 2 at Re = 900 was calculated for three sets of grid systems. The grid numbers were 2.63 million (coarse), 6.32 million (fine) and 10.01 million (finest), respectively. We can see from Fig. 3 that an increment of the grid number caused a reduction of the comparative deviations for both Nu and f. The corresponding errors between the fine and finest grid systems were 1.9% for Nu and 0.9% for f, implying that the fine grid system with 6.32 million elements ensured the accuracy of numerical simulations. Therefore, similar grid systems were employed in the following simulations.

3.3. Validation of numerical results

Simulations of the flow and heat transfer behavior in a tube with conical strip vortex generators were conducted to check the present numerical results. The calculated Nu/Nu_0 and f/f_0 were compared with those of experiments as documented in [24]. Note that the physical model and boundary conditions used in the simulations, and experiments were the same. As shown in Fig. 4, the present numerical results were in good accordance with the experimental results. The maximum differences for Nu/Nu_0 and f/f_0 were less than 14% and 11%, respectively. Because the uncertainties for Nu and f measurements during experiments were 14.4% and 10.3%, respectively, the deviations between numerical results and experimental data could be ascribed to uncertainty during measurements, demonstrating that the present numerical results are convincing.

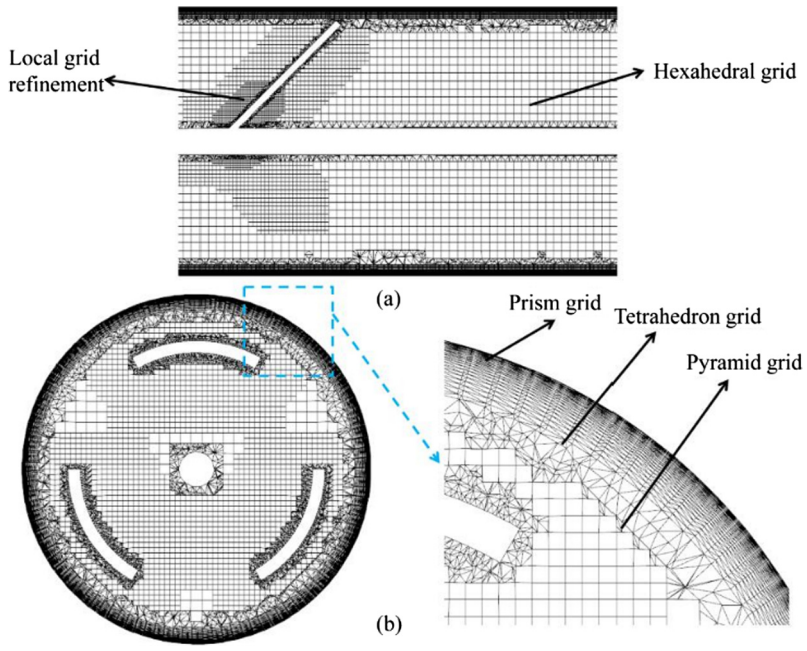

Fig. 2. Grid generation for the computational domain.

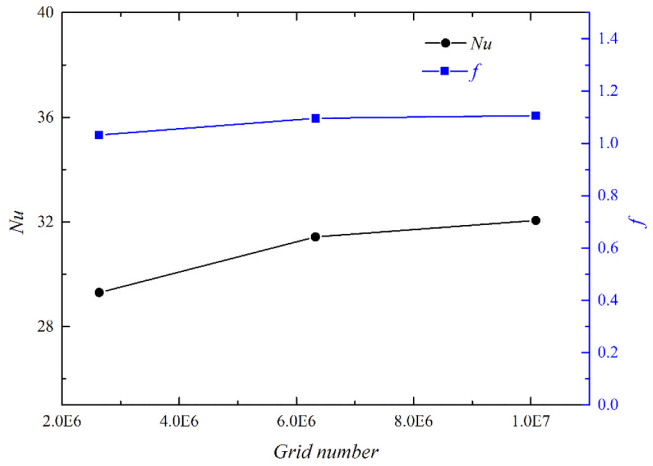

Fig. 3. Grid independence test.

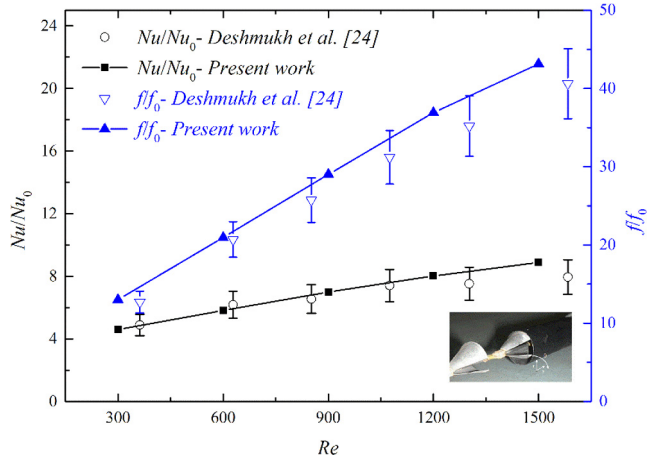

Fig. 4. Comparison of Nu/Nu_0 and f/f_0 between numerical results and experimental data [24] in a tube fitted with conical strip vortex generators.

4. Response Surface Methodology (RSM)

In this work, we applied the Response Surface Methodology (RSM) to find an adaptive approximation for the functional relationship between the output and input variables by numerical experiments and analysis. The second-order RSM model considering the entire linear, square, and interaction terms were used for approximating the response, and the general form of the model is given by:

$$y = N_0 + \sum_{i=1}^{n} N_i x_i + \sum_{i=1}^{n} N_{ii} x_i^2 + \sum \sum_{i<j} N_{ij} x_i x_j + \varepsilon \quad (10)$$

Based on the initial study of this paper, the input parameters or design parameters considered were *Re*, *C*, and P^*, and the responses or objective functions were Nu/Nu_0 and f/f_0. The input parameters were chosen in three levels. To design the experiments, a central composite design (CCD) was used for fitting the second-order models. Table 1 displays the arrangements of the runs of simulation regarding both coded values and real values based on the CCD. The values of (−1), (0), (1) in the table mean the low, middle and high levels of the variable, respectively.

5. Results and discussion

5.1. Model estimation

After finishing the runs of numerical simulation, the obtained Nu/Nu_0, and f/f_0 were presented in Table 1. These responses were then utilized to find the coefficients of the second-order model. Accuracy and significance of the coefficients were tested through the analysis of variance (ANOVA) using the commercial software Minitab 16.0. Tables 2 and 3 show the results of ANOVA for Nu/Nu_0 and f/f_0, respectively.

In Tables 2 and 3, the degree of freedom (*DOF*) is equal to the number of levels of the variable minus one. The total sum of squares (*SS*) helps express the total variation attributed to various factors, and *Seq. SS* means the sequential sums of squares, and *Adj. SS* represents the adjusted sums of squares. The mean square (*MS*)

Table 1
The design of experiment.

Run order	Coded value			Real value			Response	
	Re	*C*	P^*	*Re*	*C*	P^*	Nu/Nu_0	f/f_0
1	−1	0	0	300	1/2	3	4.39	5.61
2	0	−1	0	900	1/3	3	5.57	7.25
3	−1	1	1	300	2/3	4	4.69	6.96
4	0	0	0	900	1/2	3	6.66	11.4
5	−1	−1	−1	300	1/3	2	4.29	4.80
6	0	0	1	900	1/2	4	6.60	9.23
7	1	−1	1	1500	1/3	4	6.34	8.17
8	−1	−1	1	300	1/3	4	3.64	3.17
9	0	0	0	900	1/2	3	6.66	11.4
10	0	0	−1	900	1/2	2	7.21	15.41
11	1	1	−1	1500	2/3	2	9.591	38.53
12	0	0	0	900	1/2	3	6.66	11.4
13	1	0	0	1500	1/2	3	8.28	16.44
14	0	0	0	900	1/2	3	6.66	11.4
15	1	1	1	1500	2/3	4	8.48	21.46
16	0	1	0	900	2/3	3	7.73	18.6
17	−1	1	−1	300	2/3	2	5.26	11.9
18	1	−1	−1	1500	1/3	2	7.81	13.17
19	0	0	0	900	1/2	3	6.66	11.4
20	0	0	0	900	1/2	3	6.66	11.4

Table 2
The results of ANOVA for Nu/Nu_0.

Source	*DOF*	*Seq. SS*	*Adj. SS*	*Adj. MS*	*F-value*	*P-value*
Regression	9	43.3889	43.3889	4.821	152.91	0
Linear	3	41.6897	41.6897	13.8966	440.76	0
Re	1	33.1768	33.1768	33.1768	1052.29	0
C	1	6.5679	6.5679	6.5679	208.32	0
P^*	1	1.9449	1.9449	1.9449	61.69	0
Square	3	0.9848	0.9848	0.3283	10.41	0.002
ReRe	1	0.9216	0.5237	0.5237	16.61	0.002
CC	1	0.0158	0.0393	0.0393	1.25	0.29
P^*P^*	1	0.0474	0.0474	0.0474	1.5	0.248
Interaction	3	0.7144	0.7144	0.2381	7.55	0.006
ReC	1	0.4552	0.4552	0.4552	14.44	0.003
ReP^*	1	0.2334	0.2334	0.2334	7.4	0.022
CP^*	1	0.0257	0.0257	0.0257	0.82	0.388
Residual error	10	0.3153	0.3153	0.0315	–	–
Lack-of-fit	5	0.3153	0.3153	0.0631	–	–
Pure error	5	0	0	0	–	–
Total	19	43.7042	–	–	–	–

R^2 = 99.28%, R^2 (Predicted) = 94.41%, R^2 (Adjusted) = 98.63%.

Table 3
The results of ANOVA for f/f_0.

Source	*DOF*	*Seq. SS*	*Adj. SS*	*Adj. MS*	*F-value*	*P-value*
Regression	9	1094.78	1094.78	121.642	89.78	0
Linear	3	918.5	918.5	306.168	225.96	0
Re	1	426.71	426.71	426.71	314.93	0
C	1	370.6	370.6	370.605	273.52	0
P^*	1	121.19	121.19	121.189	89.44	0
Square	3	20.37	20.37	6.792	5.01	0.022
ReRe	1	6.46	0.34	0.341	0.25	0.627
CC	1	11.5	6.56	6.558	4.84	0.05
P^*P^*	1	2.41	2.41	2.414	1.78	0.212
Interaction	3	155.9	155.9	51.966	38.35	0
ReC	1	96.31	96.31	96.308	71.08	0
ReP^*	1	30.06	30.06	30.057	22.18	0.001
CP^*	1	29.53	29.53	29.533	21.8	0.001
Residual error	10	13.55	13.55	1.355	–	–
Lack-of-fit	5	13.55	13.55	2.71	–	–
Pure error	5	0	0	0	–	–
Total	19	1108.33	–	–	–	–

R^2 = 98.78%, R^2 (Predicted) = 76.98%, R^2 (Adjusted) = 97.68%.

is the sum of squares divided by the degrees of freedom. The *F-value* is a measure of variance of data about the mean, and a higher *F-value* indicates a more significant effect. The *P-value* means a probability that determines the evidence against the null hypothesis, and a lower *P-value* provides a stronger evidence against the null hypothesis. Besides, R^2 is the coefficient of determination or multiple determination. Usually, a higher R^2 means that the model fits the data better. R^2 (Predicted) is used to determine how well the model predicts responses for new observations, and R^2 (Adjusted) means the adjusted coefficient of determination. More details about statistical estimators for analysis of variance are available in [25].

As shown in Table 2, the value of R^2 for the regression model was 99.28%, intending that the model could not embody only 0.72% of total change. The high meaningfulness of the present model was reflected by the large *F-value* of 152.91, which is far more than the unity. Furthermore, statistical analysis was conducted based on the *P-value* with 95% certainty to determine whether the model terms were significant or not. Note that the terms with *P-value* less than 0.05 are important for the model and the terms with *P-value* larger than 0.05 are insignificant, which should be neglected. In this sense, it was found from Table 2 that the linear terms of the *Re*, *C*, and P^*, the square terms of *ReRe*, together with the interaction terms of *ReC* and *ReP* were the valid terms related to the Nusselt number ratio. However, the square terms of *CC* and P^*P^* and the interaction term of CP^* presented a meaningless influence. Besides, the significance level regarding the *F-value* of the mentioned meaningful terms for the Nusselt number ratio from low to high was the interaction terms, the square terms, and the linear terms. Moreover, among model terms affecting the Nusselt number ratio, the linear term of *Re* was the most significant one.

According to the results for the friction factor ratio as shown in Table 3, the value of R^2 for the regression model was 98.78%, suggesting that the model could embody 98.78% of total change. The high *F-value* of 89.78 and the low *P-value* implied that the present regression model was significant. According to the *P-values*, all the model terms were meaningful to the friction factor ratio except the interaction terms of *ReRe* and P^*P^*. Moreover, the meaningfulness level regarding the *F-value* of the mentioned meaningful model terms for the friction factor ratio from low to high was the square terms, the interaction terms, and the linear terms, and the linear term of *Re* was the most significant model term for the friction factor ratio.

The residual plots for Nu/Nu_0 and f/f_0 achieved by the analysis of variance were also presented in Figs. 5 and 6. Usually, a residual is the difference between an observed value and its corresponding fitted value, and a residual plot is a graph that is used to examine the goodness-of-fit in regression and ANOVA. The residual plots presented in Figs. 5 and 6 included the normal probability plot of residuals, histogram of the residuals, residuals versus fits and residuals versus order of data. The objective of examining residual is to determine whether the RSM model used in this work is adequate.

The normal probability plots of residual distributions were displayed in Figs. 5 and 6 to examine the normality of the observation. We can see that the diagrams of normal probability were straight lines, which imply that the residual distributions for both Nu/Nu_0 and f/f_0 are normal. To determine whether the data are skewed or whether outliers exist in the data, the histogram of the residuals were presented. It is evident that the residual histogram for f/f_0 presented a symmetrical distribution while the residual histogram for Nu/Nu_0 had skewed distribution, but as a whole, it approached a symmetrical distribution. One sees from the residuals versus fits plots in Figs. 5 and 6 that the maximum residuals were within 0.73 and 1.58 for Nu/Nu_0 and f/f_0, respectively, and the residuals roughly formed a horizontal band around the zero line, implying that the variances of the error terms are equal. In addition, it was found that all the residuals were within the basic random pattern of residuals, which suggests that there are no outliers. The residuals versus order plots for Nu/Nu_0 and f/f_0 were also presented in Figs. 5 and 6. It is clear that the residuals for Nu/Nu_0 and f/f_0 bounced randomly around the zero line, suggesting that the residuals are uncorrelated with each other. Therefore, it can be concluded that the present RSM model has reasonable accuracy.

By RSM, we finally achieved the estimated coefficients for Nu/Nu_0 and f/f_0. Note that the meaningless model terms were neglected, and only the significant terms were adopted. The specific functional relationships between responses and input variables as coded units are given as follows.

$$Nu/Nu_0 = 6.7042 + 1.8214Re + 0.8104C - 0.4410P^* - 0.4364ReRe + 0.2385ReC - 0.1708ReP^* \quad (11)$$

$$f/f_0 = 11.3885 + 6.5323Re + 6.0877C - 3.4812P^* + 1.5442CC + 3.4696ReC - 1.9383ReP^* - 1.9214CP^* \quad (12)$$

5.2. Sensitivity analysis

Sensitivity analysis, which is a method to determine how the uncertainties in a model input affect the output for the model, were conducted in the present work. The partial derivatives of Nu/Nu_0 and f/f_0 respect to certain effective parameter were calculated as their sensitivity. The partial derivatives of Nu/Nu_0 and f/f_0 are expressed in the following.

$$\frac{\partial(Nu/Nu_0)}{\partial Re} = 1.8214 - 0.8728Re + 0.2385C - 0.1708P^* \quad (13)$$

$$\frac{\partial(Nu/Nu_0)}{\partial C} = 0.8104 + 0.2385Re \quad (14)$$

$$\frac{\partial(Nu/Nu_0)}{\partial P^*} = -0.4410 - 0.1708Re \quad (15)$$

$$\frac{\partial(f/f_0)}{\partial Re} = 6.5323 + 3.4696C - 1.9383P^* \quad (16)$$

$$\frac{\partial(f/f_0)}{\partial C} = 6.0877 + 3.0884C + 3.4696Re - 1.9214P^* \quad (17)$$

$$\frac{\partial(f/f_0)}{\partial P^*} = -3.4812 - 1.9383Re - 1.9214C \quad (18)$$

Table 4 presents the results of Eqs. (13)–(18). These values were obtained for the tube fitted with conical strip vortex generators with *Re* at levels of −1 and 0 (300 and 900), *C* at levels of -1, 0 and 1 (1/3, 1/2 and 2/3) and P^* at levels of −1, 0 and 1 (2, 3 and 4). Note that the positive value in the table indicates an increase of input parameters results in an increment in output parameters while the negative value implies the opposite trend, and the larger value means the higher sensitivity. Moreover, we provided Figs. 7–9 to render the results.

As shown in Fig. 7 and Table 4, the sensitivity of Nu/Nu_0 and f/f_0 to Reynolds number was positive, indicating that an increment in Reynolds number led to an enhancement in both heat transfer and pressure drop. The reason for this phenomenon is that the mass flow rate is proportional to the Reynolds number, and an increment in Reynolds number means a higher mass flow rate so that more fluid can be used to transfer heat at a given time. At the same time, conveying more fluid will consume more pumping power. For a given pitch ratio, the sensitivity of Nu/Nu_0 and f/f_0 to

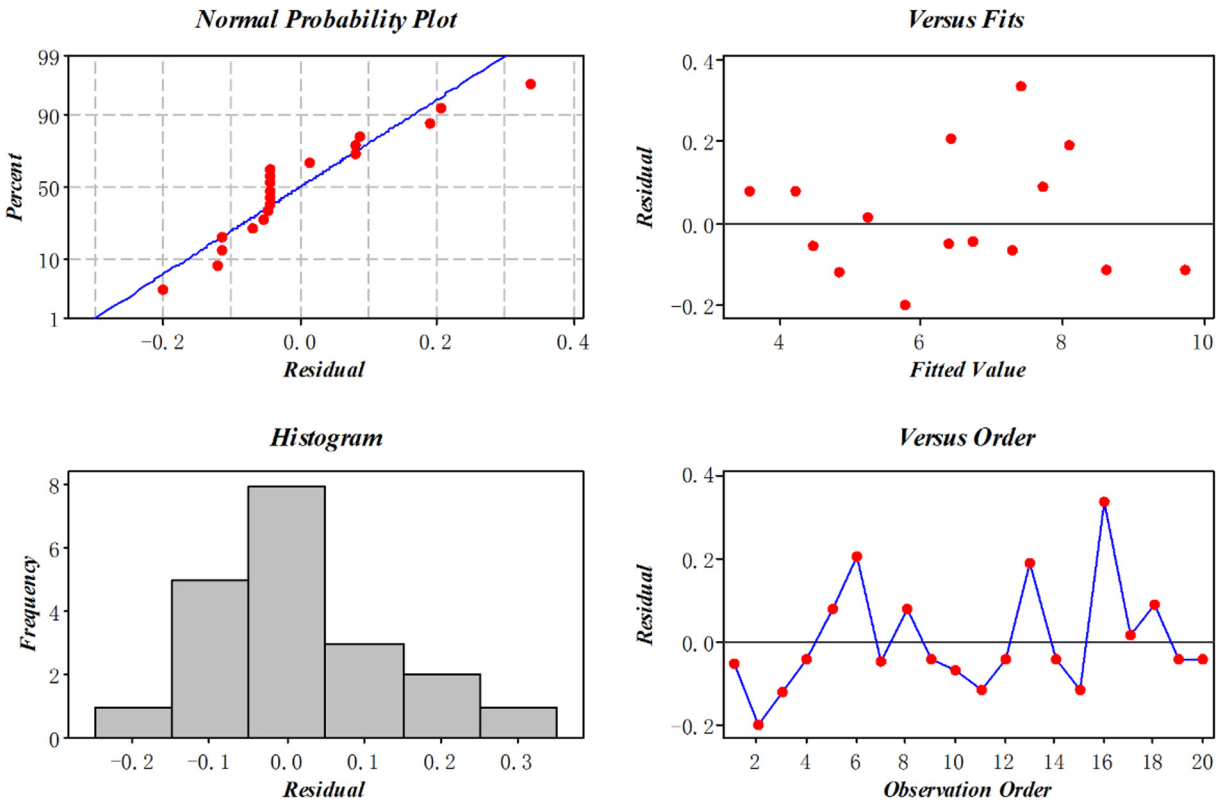

Fig. 5. Residual plots for Nu/Nu_0.

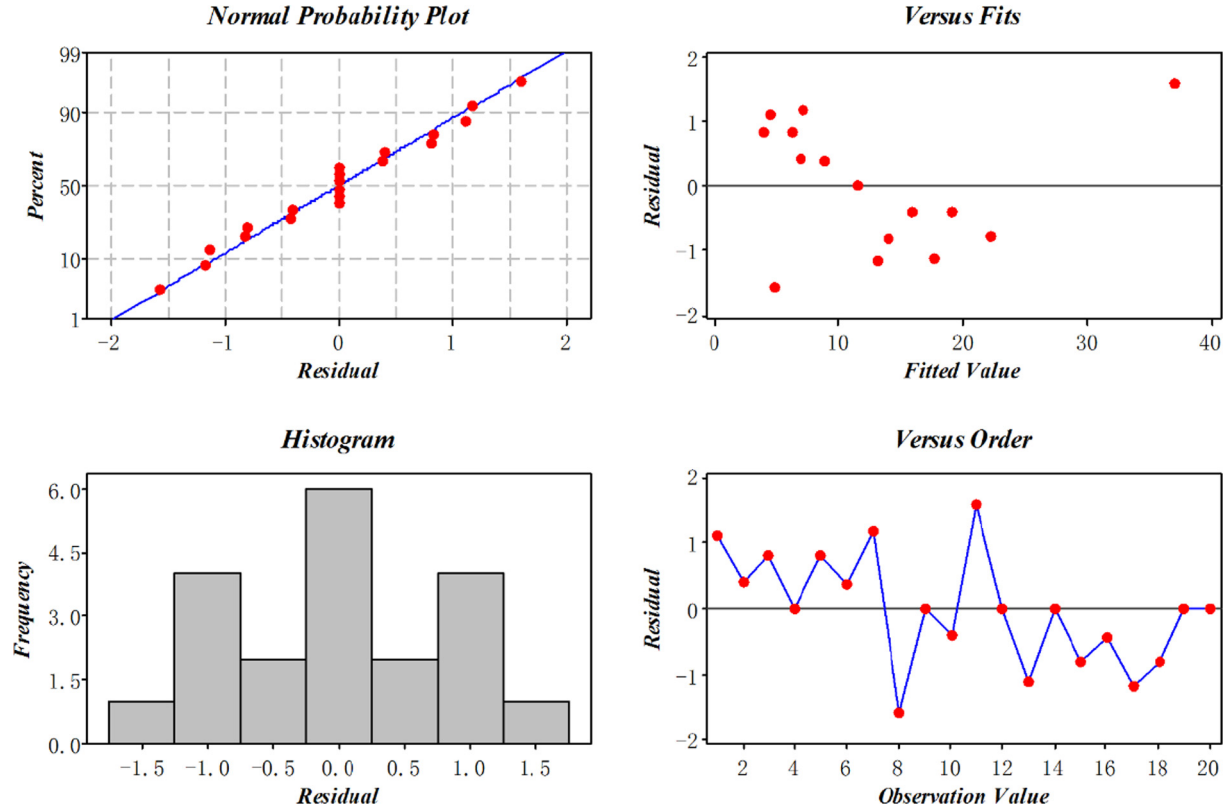

Fig. 6. Residual plots for f/f_0.

Table 4
Sensitivity analysis of Nu/Nu_0 and f/f_0.

Re	C	P^*	$\frac{\partial(Nu/Nu_0)}{\partial Re}$	$\frac{\partial(Nu/Nu_0)}{\partial C}$	$\frac{\partial(Nu/Nu_0)}{\partial P^*}$	$\frac{\partial(f/f_0)}{\partial Re}$	$\frac{\partial(f/f_0)}{\partial C}$	$\frac{\partial(f/f_0)}{\partial P^*}$
−1	−1	−1	2.6265	0.5719	−0.2702	5.001	1.4511	0.3785
−1	−1	0	2.4557	0.5719	−0.2702	3.0627	−0.4703	0.3785
−1	−1	1	2.2849	0.5719	−0.2702	1.1244	−2.3917	0.3785
−1	0	−1	2.865	0.5719	−0.2702	8.4706	4.5395	−1.5429
−1	0	0	2.6942	0.5719	−0.2702	6.5323	2.6181	−1.5429
−1	0	1	2.5234	0.5719	−0.2702	4.594	0.6967	−1.5429
−1	1	−1	3.1035	0.5719	−0.2702	11.94	7.6279	−3.4643
−1	1	0	2.9327	0.5719	−0.2702	10.002	5.7065	−3.4643
−1	1	1	2.7619	0.5719	−0.2702	8.0636	3.7851	−3.4643
0	−1	−1	1.7537	0.8104	−0.441	5.001	4.9207	−1.5598
0	−1	0	1.5829	0.8104	−0.441	3.0627	2.9993	−1.5598
0	−1	1	1.4121	0.8104	−0.441	1.1244	1.0779	−1.5598
0	0	−1	1.9922	0.8104	−0.441	8.4706	8.0091	−3.4812
0	0	0	1.8214	0.8104	−0.441	6.5323	6.0877	−3.4812
0	0	1	1.6506	0.8104	−0.441	4.594	4.1663	−3.4812
0	1	−1	2.2307	0.8104	−0.441	11.94	11.0975	−5.4026
0	1	0	2.0599	0.8104	−0.441	10.002	9.1761	−5.4026
0	1	1	1.8891	0.8104	−0.441	8.0636	7.2547	−5.4026

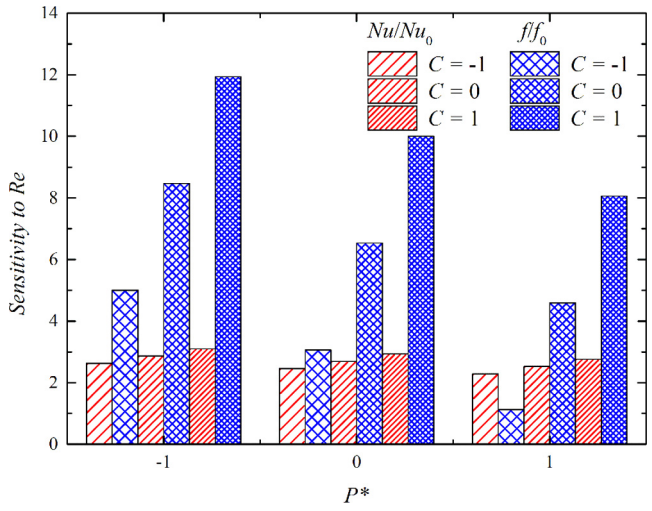

Fig. 7. The sensitivity of Nu/Nu_0 and f/f_0 to Re.

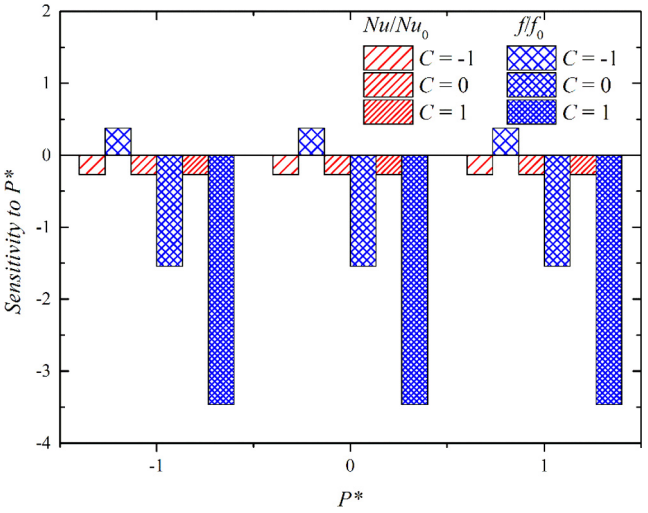

Fig. 9. The sensitivity of Nu/Nu_0 and f/f_0 to P^*.

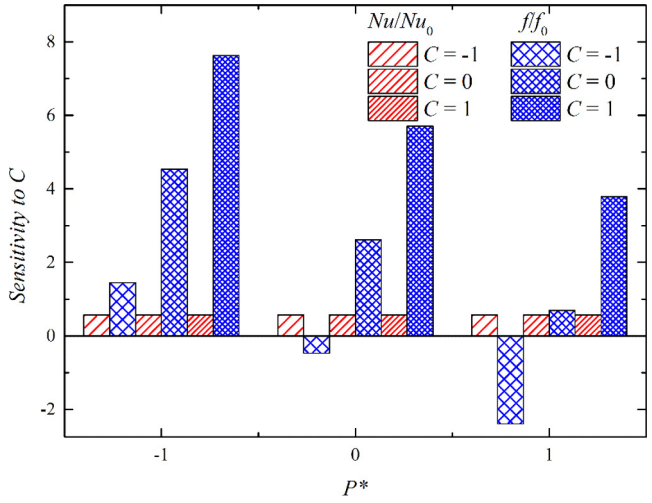

Fig. 8. The sensitivity of Nu/Nu_0 and f/f_0 to C.

Reynolds number increased with an increment of the conical strip filling ratio, and f/f_0 was more sensitive to Reynolds number compared to Nu/Nu_0. The result implies that increasing the conical strip filling ratio enhances both heat transfer and pressure drop, and the growth rate of heat transfer enhancement is less than that of pressure drop augmentation. At a constant conical strip filling ratio, the sensitivity of f/f_0 to Reynolds number decreased with an increment in the pitch ratio while the sensitivity of Nu/Nu_0 remained constant, which indicated that the sensitivity of Nu/Nu_0 to Reynolds number was not affected by the parameter pitch ratio in this case. Therefore, designers may use a larger pitch ratio to realize heat transfer enhancement with less pressure drop when the conical strip filling ratio remains unchanged.

The sensitivity of Nu/Nu_0 and f/f_0 to the conical strip filling ratio is presented in Fig. 8. Clearly, the sensitivity of Nu/Nu_0 to the conical strip filling ratio was positive, which indicated that Nu/Nu_0 rose by enlarging the conical strip filling ratio. This phenomenon can be explained by the fact that enlarging the conical strip filling ratio increases the area of the conical strips, which causes a stronger disturbance of the fluid. Compared to the sensitivity of Nu/Nu_0 to the conical strip filling ratio, the change rule and tending of the sensitivity of the f/f_0 to this parameter were a bit more complicated, especially for the parameter C at the level of −1. We can see from the figure that the sensitivity of f/f_0 to C had a positive value at the low level of the pitch ratio but it became negative with the further increment of the pitch ratio. In other cases, this sensitivity was always positive, implying that f/f_0 increased by

increasing the parameter C. The reason for this phenomenon is that enlarging the conical strip filling ratio increases the area of the conical strips, which leads to more flow blockage and thereby increases the pressure drop. Considering that fact that the flow blockage caused by the vortex generator decreases with an increase of the pitch ratio, so the growth rate of pressure drop augmentation may decrease with an increment of the conical strip ratio at a large pitch ratio. In addition, the sensitivity of f/f_0 to the conical strip filling ratio generally increased with an increment in the parameter C for a given pitch ratio, and decreased with an enhancement in the pitch ratio for a given conical strip filling ratio. Therefore, f/f_0 was more sensitive to the conical strip filling ratio, compared to Nu/Nu_0. Designers may use a larger conical strip filling ratio to enhance heat transfer, but they should pay attention to the pressure drop augmentation caused by the blockage of the vortex generator.

According to Fig. 9, the sensitivity of Nu/Nu_0 to the pitch ratio was negative, implying that an increment in the pitch ratio resulted in a reduction in Nu/Nu_0. As we know, a larger pitch ratio of the conical strip vortex generator means that the number of the vortex generators decreases within a given length so that the disturbance caused by the conical strip vortex generators will diminish. Therefore, designers may take advantage of this rule to enhance heat transfer by decreasing the pitch ratio of the conical strip vortex generators properly. In general, the sensitivity of f/f_0 to the pitch ratio decreased with an increase in the parameter C at a fixed pitch ratio. Note that this sensitivity was positive at the low level of C and it changed to be negative with the increment of the conical strip filling ratio, which meant that f/f_0 increased with an enhancement in the pitch ratio and it presented the opposite trend with higher levels of the parameter C. The phenomenon above can be attributed to the interaction between the conical strip filling ratio and the pitch ratio. As a result, designers should not only pay attention to the individual effect of the conical strip filling ratio and the pitch ratio, but also heed the interaction between them in designing conical strip vortex generator for heat transfer enhancement. At the same time, it was noticed that f/f_0 was more sensitive to the pitch ratio than Nu/Nu_0 to this parameter. Although decreasing the pitch ratio of the conical strip vortex generator properly is a method to enhance heat transfer, a too small pitch ratio will result in considerable pressure drop. Therefore, it is of significance to keep a balance between heat transfer enhancement and pressure drop augmentation by selecting a proper pitch ratio of the conical strip vortex generator in practical applications.

6. Multi-objective optimization

To determine the optimum combination of the input parameters for the maximum Nu/Nu_0 with the minimum f/f_0, we carried out a multi-objective optimization. The present problem was formulated using coded values as follows:

Maximum Nu/Nu_0;
Minimum f/f_0;
Subjected to $-1 < Re < 1, \quad -1 < C < 1, \quad -1 < P^* < 1.$

In this work, the commonly used NSGA-II [26] was employed to optimize the objective functions obtained by RSM. The optimum Pareto front was finally attained as shown in Fig. 10. Note that all the points on the Pareto front are optimal points that these points have no dominance over one another.

To select the most compromising solution from the Pareto front for industrial applications, Technique for Order Preference by Similarity to an Ideal Solution (TOPSIS) [27] was used in this work. The solution selected by TOPSIS was also shown in Fig. 10. The Nu/Nu_0 and f/f_0 for the solution chosen by TOPSIS were 6.57 and 7.07, respectively. Therefore, the best combination of input parameters for the solution was $Re = 0.9358$, $C = -0.8755$ and $P^* = 0.9725$ in coded values, or $Re = 1468$, $C = 0.35$ and $P^* = 3.97$ in real values.

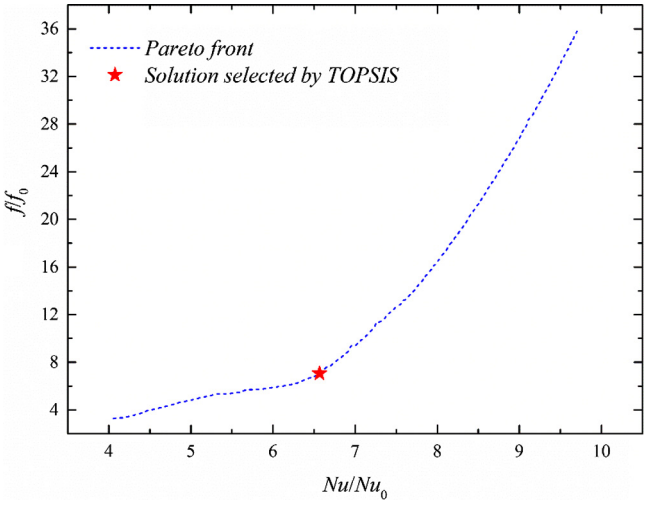

Fig. 10. Pareto front and the optimum solution selected by TOPSIS.

The superiority of the solution selected by TOPSIS was demonstrated by comparing the objective functions in different situations as displayed in Fig. 11. It was found that the maximum Nu/Nu_0 was 9.72, and the minimum f/f_0 was 3.26. The solution selected by TOSIS presented an 80% reduction in f/f_0 with only a 32% decrease in Nu/Nu_0, compared with the solution with the maximum Nu/Nu_0. Compared with the solution selected by TOPSIS, the solution with the minimum f/f_0 showed a 38% decrease in Nu/Nu_0 with only a 54% reduction in f/f_0. Therefore, the solution selected by TOPSIS was superior over the other solutions to enhance heat transfer rate with less pressure drop, and the associated design parameters for the proposed conical strip vortex generators were recommended for industrial applications.

7. Analysis of the flow and temperature fields

To understand the physical mechanism of heat transfer enhancement of the conical strip vortex generators, it is necessary to analyze the flow and temperature fields in the tube with the

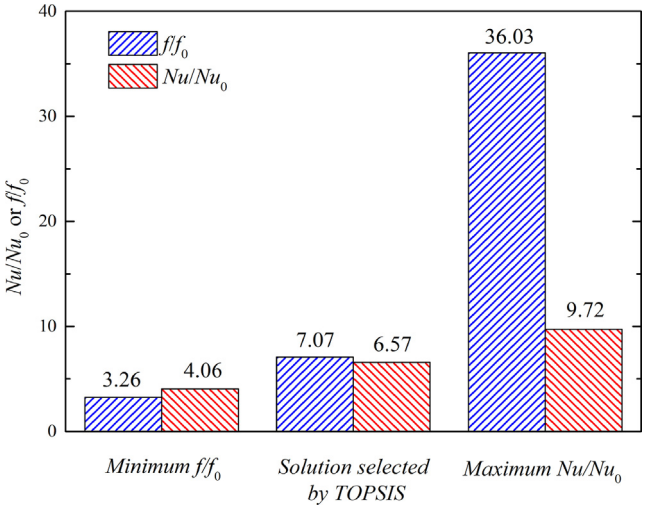

Fig. 11. Comparison of the objective functions in different situations.

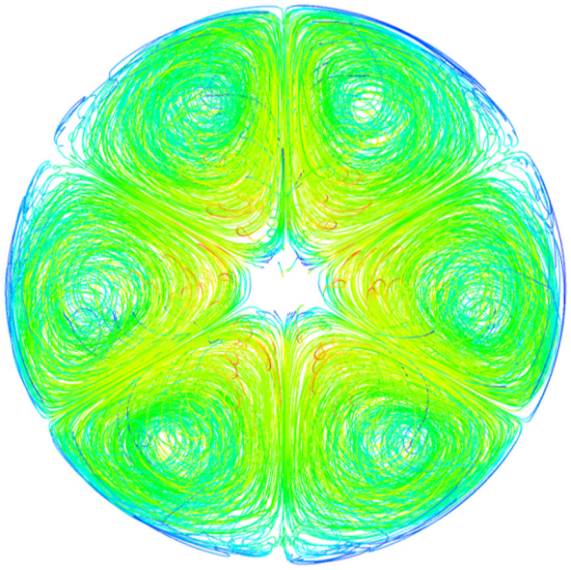

Fig. 12. Three-dimensional streamlines in the tube with the conical strip vortex generators.

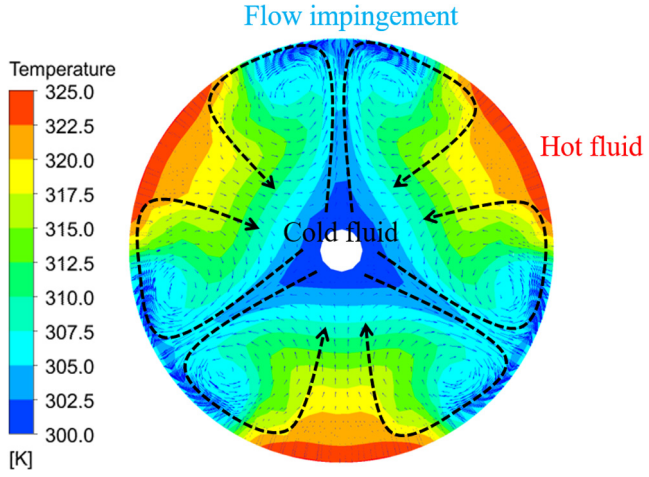

Fig. 13. Temperature contours with superimposed velocity vectors at a transverse section behind the vortex generator.

proposed vortex generators in this work. Fig. 12 presents the three-dimensional streamlines in the tube with the conical strip vortex generators. It was found that the vortex generators changed the flow filed significantly that three pairs or six longitudinal swirl flows were induced by the vortex generators in the tube. Compared to flow field in a smooth tube, these swirls helped to mix the fluid between the near wall and core flow regions, which would have an influence on the temperature distributions.

Fig. 13 presents that temperature contours with superimposed velocity vectors at a transverse section behind the vortex generator. From the velocity vectors, it was observed that three pairs or six vortexes were generated, which was in consistent with the three-dimensional streamlines. As indicated by the dotted lines, cold fluid in the core flow region was transferred towards the near wall regions and then washed against the wall, which resulted in flow impingement. The temperature in the regions where flow impingement occurred was much lower than that in the regions nearby. The reason for this is that flow impingement induced by the vortexes helps to disrupt the thermal boundary layer growth, and results in large temperature gradients near the wall, which improves the thermal performance significantly so that more heat can be taken away by the fluid. At the same time, it was observed that the heated fluid near the wall was pushed into the core flow region by the vortexes and mixed with the cold fluid. Owing to the iterative fluid mixing process, fluid between the near wall and core flow regions could be well mixed, and the better heat transfer performance was achieved finally.

8. Conclusions

In this work, we have conducted the sensitivity analysis and multi-objective optimization of a heat exchanger tube inserted with conical strip vortex generators using RSM and NSGA-II. It was found that the linear term of *Re* was the most significant one among model terms affecting the heat transfer rate and the pressure drop through the analysis of variance. Results of the sensitivity analysis indicated that increasing the conical strip filling ratio and the Reynolds number always enhanced the heat transfer rate, while increasing the pitch ratio decreased this rate. The heat transfer rate was less sensitive to the design parameters such as the Reynolds number, the conical strip filling ratio and the pitch ratio, compared to the pressure drop. Moreover, the maximum heat transfer enhancement was 9.72, and the minimum pressure drop augmentation was 3.26, but the two values could not be obtained simultaneously. The most compromising solution ($Re = 1468$, $C = 0.35$ and $P^* = 3.97$) was selected by TOPSIS from the Pareto front, and the heat transfer enhancement and the pressure drop augmentation for this solution were 6.57 and 7.07, respectively. In addition, analysis of the flow and temperature fields indicated that three pairs or six longitudinal swirl flows were induced by the vortex generation in the tube. These swirls resulted in better fluid mixing between the near wall and core flow regions, and thereby enhanced the heat transfer performance.

Acknowledgments

The work was supported by the National Key Basic Research Program of China (973 Program) (2013CB228302) and the National Natural Science Foundation of China (51376069, 51606073).

References

[1] A. Saysroy, S. Eiamsa-ard, Periodically fully-developed heat and fluid flow behaviors in a turbulent tube flow with square-cut twisted tape inserts, Appl. Therm. Eng. 112 (2017) 895–910.
[2] P. Li, Z. Liu, W. Liu, G. Chen, Numerical study on heat transfer enhancement characteristics of tube inserted with centrally hollow narrow twisted tapes, Int. J. Heat Mass Transf. 88 (2015) 481–491.
[3] L.H. Tang, W.X. Chu, N. Ahmed, M. Zeng, A new configuration of winglet longitudinal vortex generator to enhance heat transfer in a rectangular channel, Appl. Therm. Eng. 104 (2016) 74–84.
[4] A. Fan, J. Deng, J. Guo, W. Liu, A numerical study on thermo-hydraulic characteristics of turbulent flow in a circular tube fitted with conical strip inserts, Appl. Therm. Eng. 31 (2011) 2819–2828.
[5] A. Abdollahi, M. Shams, Optimization of shape and angle of attack of winglet vortex generator in a rectangular channel for heat transfer enhancement, Appl. Therm. Eng. 81 (2015) 376–387.
[6] A. Abdollahi, M. Shams, Optimization of heat transfer enhancement of nanofluid in a channel with winglet vortex generator, Appl. Therm. Eng. 91 (2015) 1116–1126.
[7] C. Liu, Y.D. Deng, X.Y. Wang, X. Liu, Y.P. Wang, C.Q. Su, Multi-objective optimization of heat exchanger in an automotive exhaust thermoelectric generator, Appl. Therm. Eng. 108 (2016) 916–926.
[8] M. Mamourian, K. Milani Shirvan, R. Ellahi, A.B. Rahimi, Optimization of mixed convection heat transfer with entropy generation in a wavy surface square lid-driven cavity by means of Taguchi approach, Int. J. Heat Mass Transf. 102 (2016) 544–554.
[9] M. Darvish Damavandi, M. Forouzanmehr, H. Safikhani, Modeling and Pareto based multi-objective optimization of wavy fin-and-elliptical tube heat exchangers using CFD and NSGA-II algorithm, Appl. Therm. Eng. 111 (2017) 325–339.

[10] M. Akbarzadeh, S. Rashidi, M. Bovand, R. Ellahi, A sensitivity analysis on thermal and pumping power for the flow of nanofluid inside a wavy channel, J. Mol. Liq. 220 (2016) 1–13.
[11] M. Mamourian, K. Milani Shirvan, S. Mirzakhanlari, A.B. Rahimi, Vortex generators position effect on heat transfer and nanofluid homogeneity: a numerical investigation and sensitivity analysis, Appl. Therm. Eng. 107 (2016) 1233–1247.
[12] M. Mamourian, K. Milani Shirvan, I. Pop, Sensitivity analysis for MHD effects and inclination angles on natural convection heat transfer and entropy generation of Al_2O_3-water nanofluid in square cavity by response surface methodology, Int. Commun. Heat Mass Transf. 79 (2016) 46–57.
[13] K. Milani Shirvan, R. Ellahi, S. Mirzakhanlari, M. Mamourian, Enhancement of heat transfer and heat exchanger effectiveness in a double pipe heat exchanger filled with porous media: numerical simulation and sensitivity analysis of turbulent fluid flow, Appl. Therm. Eng. 109 (Part A) (2016) 761–774.
[14] K. Milani Shirvan, M. Mamourian, S. Mirzakhanlari, R. Ellahi, Two phase simulation and sensitivity analysis of effective parameters on combined heat transfer and pressure drop in a solar heat exchanger filled with nanofluid by RSM, J. Mol. Liq. 220 (2016) 888–901.
[15] K. Milani Shirvan, M. Mamourian, S. Mirzakhanlari, R. Ellahi, K. Vafai, Numerical investigation and sensitivity analysis of effective parameters on combined heat transfer performance in a porous solar cavity receiver by response surface methodology, Int. J. Heat Mass Transf. 105 (2017) 811–825.
[16] K. Milani Shirvan, S. Mirzakhanlari, M. Mamourian, N. Abu-Hamdeh, Numerical investigation and sensitivity analysis of effective parameters to obtain potential maximum power output: a case study on Zanjan prototype solar chimney power plant, Energy Convers. Manage. 136 (2017) 350–360.
[17] S. Mirzakhanlari, K. Milani Shirvan, M. Mamourian, A.J. Chamkha, Increment of mixed convection heat transfer and decrement of drag coefficient in a lid-driven nanofluid-filled cavity with a conductive rotating circular cylinder at different horizontal locations: a sensitivity analysis, Powder Technol. 305 (2017) 495–508.
[18] Y. You, A. Fan, Y. Liang, S. Jin, W. Liu, F. Dai, Entropy generation analysis for laminar thermal augmentation with conical strip inserts in horizontal circular tubes, Int. J. Therm. Sci. 88 (2015) 201–214.
[19] P.W. Deshmukh, R.P. Vedula, Heat transfer and friction factor characteristics of turbulent flow through a circular tube fitted with vortex generator inserts, Int. J. Heat Mass Transf. 79 (2014) 551–560.
[20] ANSYS Fluent User's Guide 15.0, ANSYS Inc, Canonsberg, PA, 2013.
[21] J. Guo, A. Fan, X. Zhang, W. Liu, A numerical study on heat transfer and friction factor characteristics of laminar flow in a circular tube fitted with center-cleared twisted tape, Int. J. Therm. Sci. 50 (2011) 1263–1270.
[22] J. Holman, Heat Transfer, ninth ed., Boston, McGraw-Hill Inc, New York, 2002, pp. 168–169.
[23] P. Liu, N. Zheng, F. Shan, Z. Liu, W. Liu, Numerical study on characteristics of heat transfer and friction factor in a circular tube with central slant rods, Int. J. Heat Mass Transf. 99 (2016) 268–282.
[24] P. Deshmukh, S. Prabhu, R. Vedula, Heat transfer enhancement for laminar flow in tubes using curved delta wing vortex generator inserts, Appl. Therm. Eng. 106 (2016) 1415–1426.
[25] D. Freedman, R. Pisani, R. Purves, Statistics (International Student Edition), Pisani, R. Purves, 4th ed., WW Norton & Company, NY, USA, 2007, p. 720.
[26] R. Long, B. Li, Z. Liu, W. Liu, Multi-objective optimization of a continuous thermally regenerative electrochemical cycle for waste heat recovery, Energy 93 (Part 1) (2015) 1022–1029.
[27] Y. Ge, Z. Liu, W. Liu, Multi-objective genetic optimization of the heat transfer for tube inserted with porous media, Int. J. Heat Mass Transf. 101 (2016) 981–987.